The Academic
International Journal of Multidisciplinary Research

An Online Peer Reviewed / Refereed Journal
Volume 3 | Issue 5 | May 2025
ISSN: 2583-973X (Online)
Website: www.theacademic.in

Facile Synthesis and Characterization of Nanowire-like Copper Oxide Electrodes for Sensitive Electrochemical Sensing of Paracetamol

Palpandi Karuppaiah
Quality Control Data Analyst
Email: sensorpandian18@gmail.com

ARTICLE DETAILS

Research Paper

Accepted: 25-05-2025

Published: 10-06-2025

Keywords:

Copper (II) oxide; chemical precipitation, green synthesis, electrochemical detection; pharmaceutical drug analysis, physiological samples

ABSTRACT

Development of nanomaterials for efficiently detecting pharmaceutical drugs such as paracetamol (PRT) is important for industrial applications. In this study, we synthesized copper oxide nanowire (CuO NW) via simple chemical co-precipitation technique. The prepared CuO NW electrodes were coated on a glassy carbon electrode (GCE) for conducting sensitive and selective electrochemical detection of PRT. The CuO NW electrodes were systematically characterized using various spectroscopic techniques including X-ray diffraction, Fourier transform infrared spectroscopy, an energy dispersive X-ray analysis and field emission scanning electron microscopy. The electrochemical properties of CuO NW electrodes were verified using electrochemical impedance spectroscopy (EIS) and cyclic voltammetry (CV) techniques. As an electrochemical sensor, the proposed nanowire-like copper oxide-glassy carbon electrode (CuO NW/GCE) demonstrated an excellent sensitivity with a wider linear response range from 0.1 to 275.1µM. The electrode also has good sensitivity. The selectivity were tested in the presence of three different co-existing biomolecules. Finally, the CuO NW/GCE exhibits consistent durability, reproducibility, and reproducibility, which are important parameters for future development as a point-of-care device.

DOI : https://doi.org/10.5281/zenodo.15643177

1. Introduction

Transition metal oxides are crucial materials for magnetic storage media, solar energy conversion, electronics, and catalysis. Some transition metal oxides, such as zinc oxide, titanium dioxide, and iron oxide, have been proven to be potential candidates for many applications. Among all transition metal oxides, copper oxide (CuO) is categorized as a highly attractive metal oxide semiconductor material because of its superior performance in electronic and optoelectronic industrial applications such as gas sensing device fabrication, semiconductor, and thin films for photovoltaic cells [1-3]. CuO is abundantly available material and is non-hazardous. The narrow band gap energy of CuO is 2.0 eV [4]. Furthermore, the fabrication and processing of CuO entails low cost [5,6]. Several synthetic approaches have been recently reported for the preparation of different CuO nanostructures such as thermal oxidation of copper foil, hydrothermal synthesis, vapor-phase solid preparation, ultrasonic irradiation method, thermal decomposition of precursors, electrodeposition and electron beam lithography [5-11]. However, it is still challenge to develop a simple, rapid, easy to control, and energy efficient method for manufacturing CuO nanostructures with a designable morphology on a large scale. To date, various morphological CuO nanostructures have been synthesized through facile solution methods such as ribbon like-films [12], nanowires [13], nanorods [14-28], plate-like powder [19], hallow microspheres [20], 3D CuO nanorods and nanowires bundle [21,22], hierarchical flower like CuO films [6,23], and butterfly like CuO [24].

Acetaminophen or paracetamol (PRT, *N*-acetyl-p-aminophenol) is widely utilized as an analgesic and antipyretic agent [25,26]. It is suitable alternative for aspirin as a pain reliever associated with a headache, backache, arthritis, and post-operative pain [27,28]. In general PRT seems to be dangerous even when consumed in normal therapeutic doses and may create serious side effects such as hepatotoxicity and nephrotoxicity, which are related to liver and kidney damage [29,30]. Therefore, the development of a simple, a fast, a sensitive, and an accurate method for the determination of PRT is crucial for quality control in pharmaceutical and overdose diagnosis [29-32].

Numerous techniques have been utilized for quantifying PRT in biological fluids and pharmaceutical formulations such as chromatography [33], capillary electrophoresis [34], spectrophotometry [35], flow injection methods [36], and electroanalytical techniques [29-32]. The electrochemical technique is more efficient than all aforementioned methods and is the most widely applied because it has the following

characteristics: higher sensitivity, good selectivity, quick response, easier to operate, and inexpensive [29-32, 37-41, 60-62].

In the present research paper, we report a facile chemical precipitation method for large-scale production of CuO NWs. For the first time we have attained this approach to prepare nanowire-like copper oxide nanostructures without using modifiers and surfactants and so on.

The formation of CuO NW reaction mechanism was detailed. We have fabricated the CuO NW modified glassy carbon electrode without utilizing of linkers and the paracetamol electrochemical sensing properties of CuO NW/GC electrodes were systematically studied.

2. Experimental Details

2.1. chemicals and instrumentation

Copper sulfate pentahydrate ($CuSO_4.5H_2O$), sodium hydroxide (NaOH), paracetamol (PRT), Bovine serum albumin (BSA), sodium phosphate dibasic and monobasic were purchased from Sigma-Aldrich. All the chemicals were used as received, and phosphate buffer was prepared using purified water. The as-synthesized compound was well characterized by using the pattern obtained from an X-ray diffractometer (PAN analytical, Netherlands), field emission scanning electron microscope (JSM-7610F), and an energy dispersive X-ray analyzer (EDX-HORIBA EMAXX-ACT). Impedance studies were conducted utilizing an electrochemical impedance spectroscope (EIM6ex Zahner, Germany). The cyclic voltammetric studies were conducted using equipment from CH instruments, USA. An electrochemical analyzer (CHIi205A, CH instruments) was employed for conducting cyclic voltammogram and differential voltammetry measurements.

2.2. Synthesis of CuO NW

Copper oxide nanowire (CuO NW) electrodes were synthesized through a simple chemical co-precipitation method [45]. Firstly, 0.6M (4.788g) of $CuSO_4.5H_2O$ was dissolved in 50-mL purified water. Moreover, 0.6M of (1.999g) sodium hydroxide (NaOH) was dissolved in 50-mL purified water individually. Then, both the solutions were mixed in a round-bottomed flask by conducting magnetic stirring at 400 rpm for 4 h. subsequently, NaOH was added in a drop-wise manner (5mL/min) with constant stirring. To maintain the pH ranges from 9.5 to 12.0 at an ambient temperature (25°C±). The resulting as-prepared solution was performed to sedimentation for 24h, and the obtained brown precipitate

was consecutively washed with water until the pH reach at 7.0. Then, ethanol (75%) was used to purified precipitate, and the mixture was centrifuged at 4000rpm for 30 min. Subsequently, the obtained products were dried at 60°C in a hot air oven for consecutive 6h. Afterwards, the product was calcined at 400°C for 2h and finely pulverized using an agate mortar with pestle. Eventually, the electrochemical studies were conducted at room temperature on the prepared sample. The **Scheme 1** explored the preparation of CuO NW and its electrochemical oxidation of PRT on CuO NW/GCE. The formation of CuO NW and chemical reaction is written in the equations (1 and 2),

$$CuSO_4 .5H_2O_{(aq)} + NaOH_{(aq)} \rightarrow Cu(OH)_{2(S)} + Na_2SO_{4(aq)} \rightarrow \quad \textbf{(1)}$$

$$Cu(OH)_{2(S)} \xrightarrow{\Delta} CuO_{(S)} + H_2O \rightarrow \textbf{(2)}$$

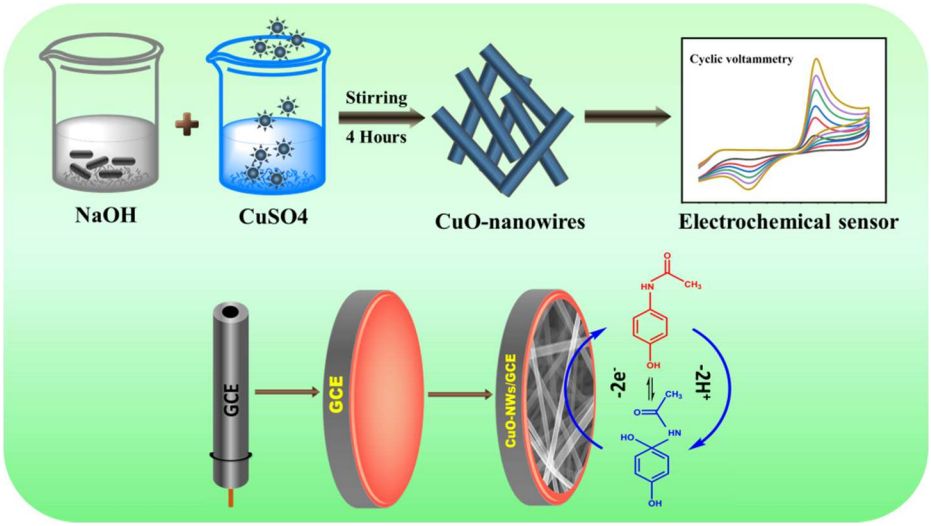

Scheme 1. Synthesis of CuO-nanowire and its electrochemical oxidation of PRT at CuO NW/GCE.

2.3. Preparation of nanowire-like CuO modified glassy carbon electrode (CuO-NW/GCE)

To fabricate a PRT sensor, initially, the naked surface of glassy carbon electrode (GCE) was cautiously polished with 0.05 µM alumina slurry by means of micro-cloth pads, and was thoroughly rinsed with double distilled water until the shining surface was obtained [42]. There any substances that are adsorbed at the electrode surface were then removed by ultrasonic treatment for 5 min and dried at ambient temperature. Moreover, about 3 mg of CuO-NW was dispersed in 1-mL of water, and sonicated for 30 min to form homogeneous suspension. Then, 8 µL suspension of CuO NW was drop coated on the cleaned surface of the GCE. Subsequently, the GCE was dried in an oven at 55°C for 5 min.

2.4. Real sample preparation (Bovine serum albumin)

A refrigerator was utilized to store Bovine serum albumin (BSA) real sample. The known amount of PRT solution were spiked into 10mL of volumetric flask containing bovine serum albumin and shacked well for few minutes. It is kept in refrigerator at 4°C until the experiments. To quantify the PRT sample content, the standard addition method was implemented using cyclic voltammetry technique (CV) in presence of 0.1M PB solution, pH at 7.0. These analyses were conducted at an ambient temperature condition.

2.5. Measurement of PRT

The electrocatalytic performance of CuO NW/GCE toward the oxidation of PRT was investigated through CV tests containing 0.1 M PB solution (pH 7.0) at a scan rate of 0.05 V s^{-1} at room temperature. Various concentrations of PRT ranging from 25 to 150 µM were detected using the developed electrode, and the linear plot was used to determine the peak current (µA) *versus* the PRT concentration (µM). To sustain the stability of the electrode, it is kept in a refrigerator at 4°C in presence of 0.1M PB solution.

3. Results and Discussion

3.1. Morphological and composition analysis of CuO NW electrodes

The surface morphological features of copper oxide nanowires (CuO NW) were confirmed using field emission scanning electron microscopy (FE-SEM), and the images were recorded at different magnifications (Fig.1). Fig.1 (A) and (B) displays the FE-SEM micrographs of CuO NW at blow magnification (x15, 000 and x35, 000) before calcination. The pre-calcined product shows the uniform structure comprising bundles of crushed leaf-like structures in huge quantities ranging from ≈0.6 to 1.0µM. The FESEM images of CuO NW electrodes represented in Fig.1 (C) and (D) were captured at magnifications of x50, 000 and x65, 000, respectively. These images revealed a bundle of huge quantities of nanowires and show the active sites of CuO NW electrodes. The average size of CuO NW was 100nm, a single wire diameter is 1.32nm and the length of a wire is 56.32nm respectively.

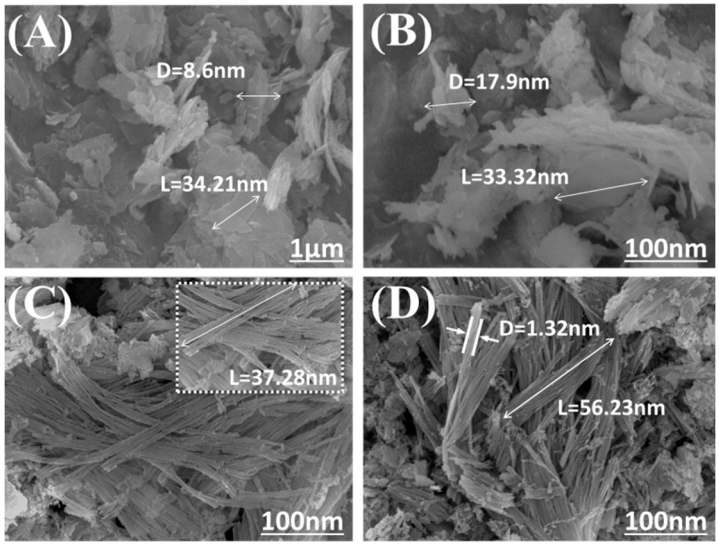

Fig. 1. FESEM morphograph of as-synthesized CuO NW before (A-B) and after calcifications (C-D).

Simultaneously, an energy dispersive X-ray (EDS) analysis was used to evaluate the CuO NW materials purity, the determination of elemental composition consisting within the materials before and after calcination process, as depicted in Fig. 2. From CuO NW EDS spectrum, the presence of copper and oxygen elements in the CuO NW electrode were confirmed. These data indicated that the nanoparticles are merely stoichiometric (Fig. 2 (A)), and the weight percentages of Cu and O in the CuO NWs, calculated using EDS results were 30.09% (Oxygen) and 69.91% (Copper) before calcination. The Fig.2 (B) reveals the after calcination of CuO NW electrode EDS data, which shows the copper and oxygen percentages i.e. 77.33 at% (Cu) from stoichiometry and 22.67 at% (O) from stoichiometry, correspondingly, which are in close proximity to the values expected, hence proving the formation of CuO NWs.

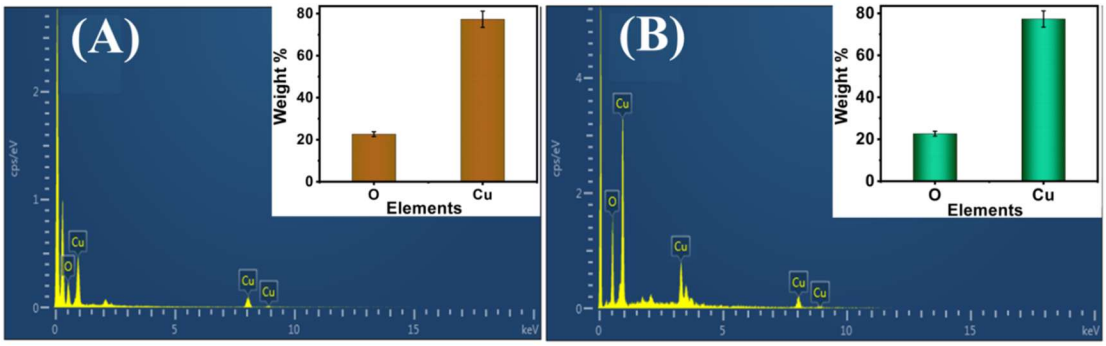

Fig. 2. EDS spectrum of as-synthesized CuO NW before (A-C), and after calcifications (D-F).

To determine the location of copper and oxygen, an elemental mapping was carried out. The results show in Fig. 3. From the Fig. 3. (A-C) and (D-F), the copper (Cu) and oxygen (O) elements are localized within the CuO NW electrodes before and after calcination was confirmed.

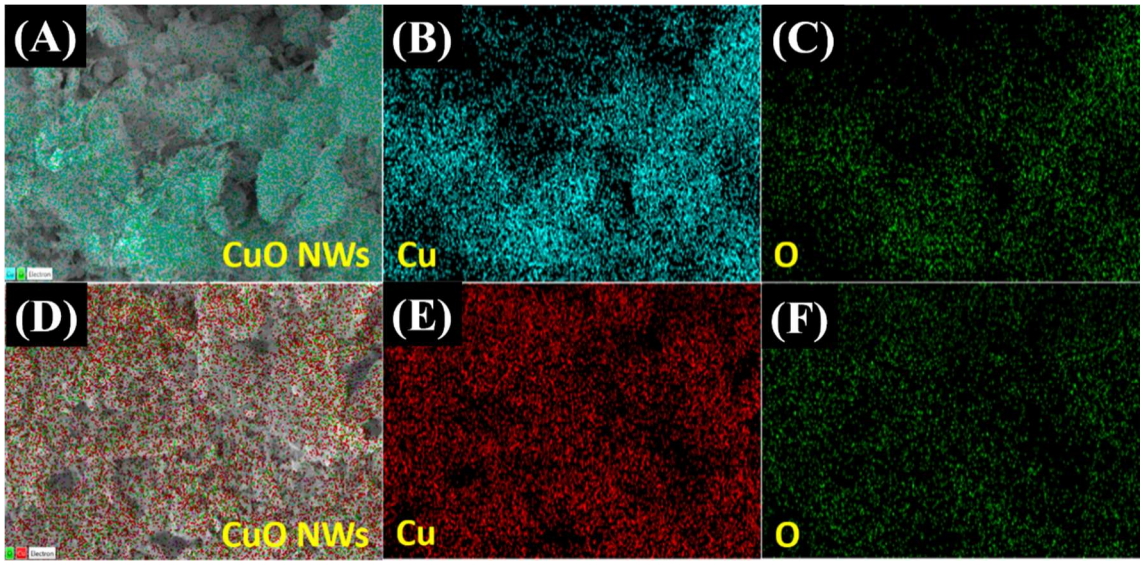

Fig. 3. Elemental mappings of CuO NW before calcination (A-C) and after calcination (D-F)

3.2. Crystalline structure analysis of CuO NW electrodes

The crystalline structure and phase purity of CuO NW electrodes were characterized by using X-ray diffraction (XRD). Fig.4. (A) represents the XRD pattern of $Cu(OH)_2$ complex obtained after drying the precipitate at 50°C. the diffraction peaks found at 32.46°, 35.51°, 38.71°, 44.75°, 53.44°, and 58.29° corresponding to the $(\bar{1}10)$,$(\bar{1}11)$, (022), (111), (150), (020), and $(\bar{1}13)$ planes of the orthorhombic Cu(OH)2, respectively, (JCPDS 80-0656). The XRD patterns of CuO NW after annealing at 400°C, all the diffraction peaks were observed and compared with the peaks in the standard data [43]. Fig.4 (B) shows the major peaks at 2θ values of 32.75°, 35.55°, 38.85°, 48.75°, 53.85°, 61.55°, 66.45°, 68.15°, 72.45°, and 74.85° that correspond to the (110), $(\bar{1}11)$, (200), $(\bar{2}02)$, (020), (202), $(\bar{1}13)$, (220), (311), and (004) planes respectively. These XRD patterns can be attributed to the monoclinic CuO NW crystal, which is in agreement with the standard JCPDS data (ref no: 5-0661). No other characteristic peaks of impurities such as $Cu(OH)_2$, Cu_2O, or precursors were observed, thus indicating the formation of a pure phase CuO NW electrodes. The average crystalline of CuO NW was examined using the full-width half maximum (FWHM) value of prominent diffraction peak of the XRD pattern through Scherer's equation (3) as follows [44]:

$$X_s = k\lambda|\beta \cos\theta \quad \rightarrow \qquad (3)$$

Where Xs is the size of the crystal, λ is denoted as wavelength of X-ray, ß is the FWHM of the diffraction peak, θ is the angle of diffraction, and k is Scherer's constant. The crystal size was calculated from the diffraction plane (111), and the average crystalline size of the CuO NW was found to be 20.1nm. The experimental results were similar to the diffraction patterns of CuO NW electrodes reported in a previous literature [45].

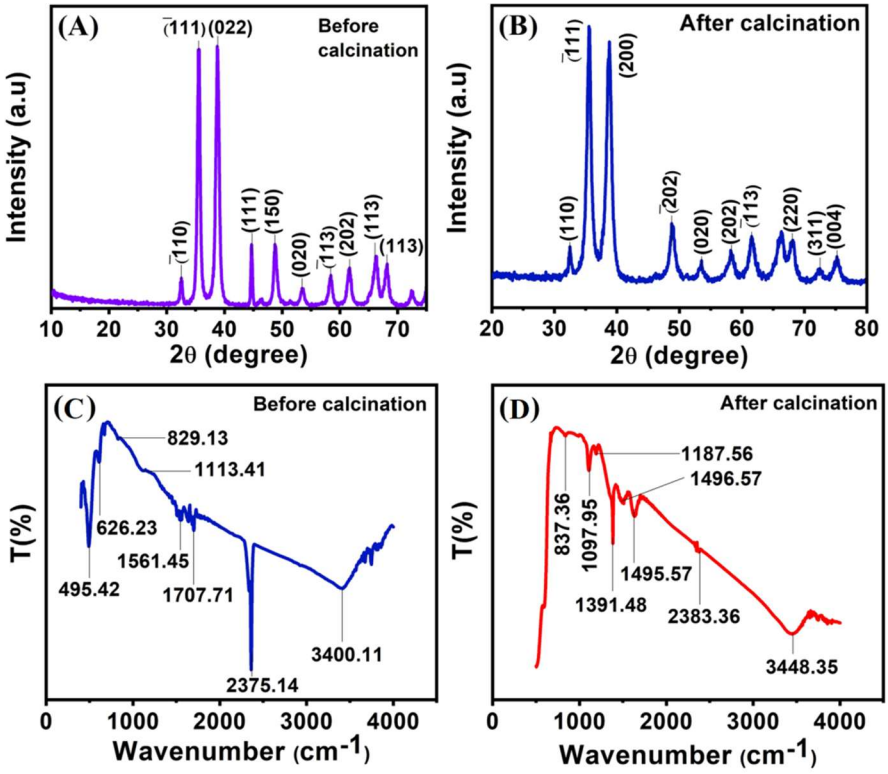

Fig. 4. XRD profiles of as-synthesized CuO NWs (A) before and (B) after calcifications and the FTIR spectrum of as-prepared nanostructures (C-D)

To determine the chemical and structural nature of the synthesized $Cu(OH)_2$ and CuO NW electrodes, the effect of chemicals used, fourier transform infrared spectroscopy (FTIR) analysis was used. Fig. 4 (C) and (D) represent the IR spectrum recorded for the $Cu(OH)_2$ and CuO NWs, respectively, in the range of 500-4000 cm^{-1} before and after calcination. In the as-synthesized $Cu(OH)_2$, the presence of peak at 3400.11 cm^{-1} indicates the stretching mode of hydroxyl groups in $Cu(OH)_2$. The peak at found at 1707.71 cm^{-1} denotes the bending mode of absorbed water molecules in the product. In the FTIR spectrum, CuO NW's peaks observed at 837.36 and 1187.56 cm^{-1} correspond to the strong Cu-O stretching vibrations.

The peak at 1495.57 cm^{-1} attributed to C=O stretching acidic groups. Bands at 3448.35 cm^{-1} may be agreed to the Cu-OH groups as displayed in Fig.4. (D).

3.3. Electrochemical properties of CuO NW/GC electrode

The electrochemical impedance spectroscopy (EIS) results of the unmodified GCE and modified electrodes (CuO NW/GCE) in 0.1M KCl containing 5mM $Fe(CN)_6^{3-/4-}$ at room temperature were shown in Fig.5. An applied frequency range was fixed at 100MHz to 100KHz. Fig.5 displays the rate of charge transfer reaction on the surface of bare GCE and CuO NW modified GC electrode. The smaller semicircle curve of the CuO NW electrodes indicates lower impedance value, which supports easier electron transfer [46-48]. In inset Fig.5 shows the Randles equivalent circuit model. This model uses electrolyte resistance (R_s), charge transfer resistance (R_{ct}), double layer capacitance (C_{dl}), and Warburg impedance (Z_w) to fit the Nyquist plot. The semicircle portion of the EIS plot obtained for CuO NW/GCE was 2.4 times higher than that of bare GC electrode. The corresponding R_{ct} values were 98.31 for the unmodified GCE (Fig.5(a)) and 52.03 for CuO NW/GCE (Fig.5(b)) respectively. These results from the impedance analysis suggested that CuO NW electrodes are good conductive materials for constructing an electrochemical sensor.

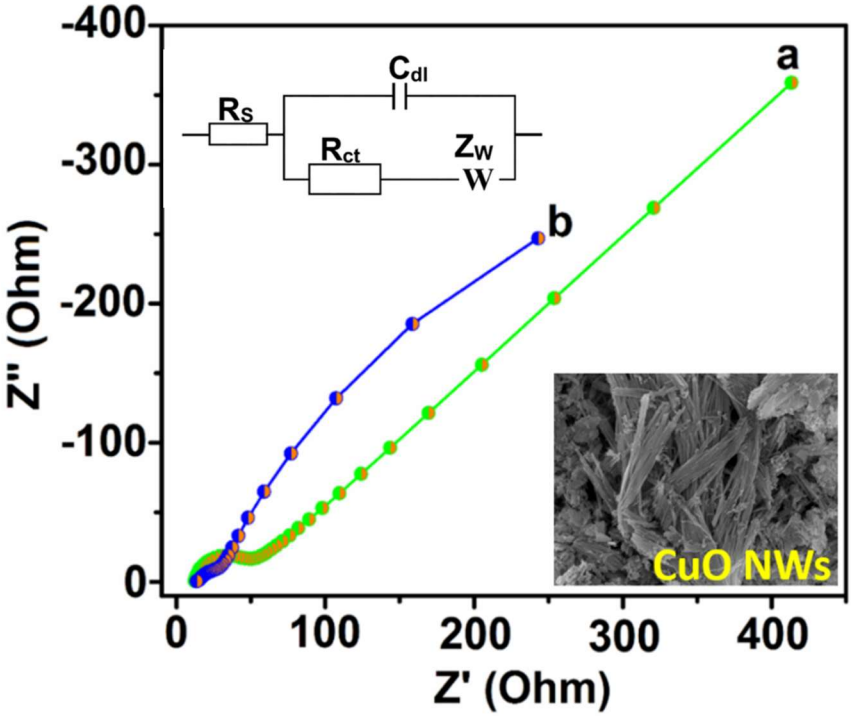

Fig.5. Typical Nyquist semicircle plots of EIS spectra. Electrode fabrication step measured in a mixture of 5mM of $Fe(CN)_6^{3-/4-}$ and 0.1M KCl solutions at an applied amplitude of ±5mV within a frequency range of 0.01Hz-100MHz. Curve (a) Bare GCE and (b) CuO NWs modified GCE. Randles equivalent circuit model is shown in inset with the corresponding FESEM image of CuO NWs.

3.4. Detection of PRT using a CuO NWs/GCE

The electrochemical oxidation properties of paracetamol (PRT) (50µM) obtained using the unmodified GCE and the CuO NW/GCE were studied utilizing 0.1M PB solution (pH 7.0) at a scan rate $0.05Vs^{-1}$ by conducting cyclic voltammetry (CV) tests. The bare GC electrode does not present any obvious redox behaviour in the presence of PRT (Fig.6A (a)), which indicates that the unmodified GCE is electrochemically inactive and it is not favorable for the detection of PRT in the selected potential range. Conversely, when the unmodified GCE was grown with CuO NWs (50µM PRT), a quasi-reversible redox behaviour with the oxidation and reduction peak potentials of 0.49V (E_{pa}) and 0.06V (E_{pc}), respectively, was obtained (Fig.6A (b)). The redox peak current of PRT obtained using CuO NW/GCE was due to the oxidation and reduction processes that occurred, because of two electrons and one proton transfer. The possible electrocatalytic redox mechanism of PRT at CuO NW/GCE is illustrated in the **Scheme 2**. Moreover, the redox peak current obtained by CuO NW modified electrodes is 6.5- fold higher than that of bare GCE. This result proved that the CuO NW/GCE had excellent electrocatalytic activity. The catalytic features of the sensor may be due to their unique properties of CuO NW electrodes, such as high volume ratio, large surface area and subtle electronic characters. Furtherly, the catalytic properties of this sensor device was confirmed by conducting CV analysis by varying the concentration of PRT ranges from 25 to 150µM in the presence of 0.1M PB solution (pH 7.0) at a sweep rate of $0.05Vs^{-1}$, as shown in Fig. 6 (B). The corresponding linear plot obtained from the relationships of redox peak current versus PRT concentration is depicts in Fig.6. (C). from this plot, the redox peak current significantly increases with increasing of concentrations. To calculate the limit of detection, selectivity and sensitivity, the CuO

NW/GCE was selected as a working electrode for further electrochemical investigations, and the oxidation peak was utilized as the analytical signal in differential pulse voltammetry (DPV) tests due to its higher sensitivity. The electrochemical oxidation reaction was takes place at the modified electrode surface is represented as the equation (4) as follows:

$$2Cu^{2+} + C_8H_9NO_2 \rightarrow 2Cu + C_8H_7NO_2 + 2H^+ \qquad \rightarrow (\mathbf{4})$$

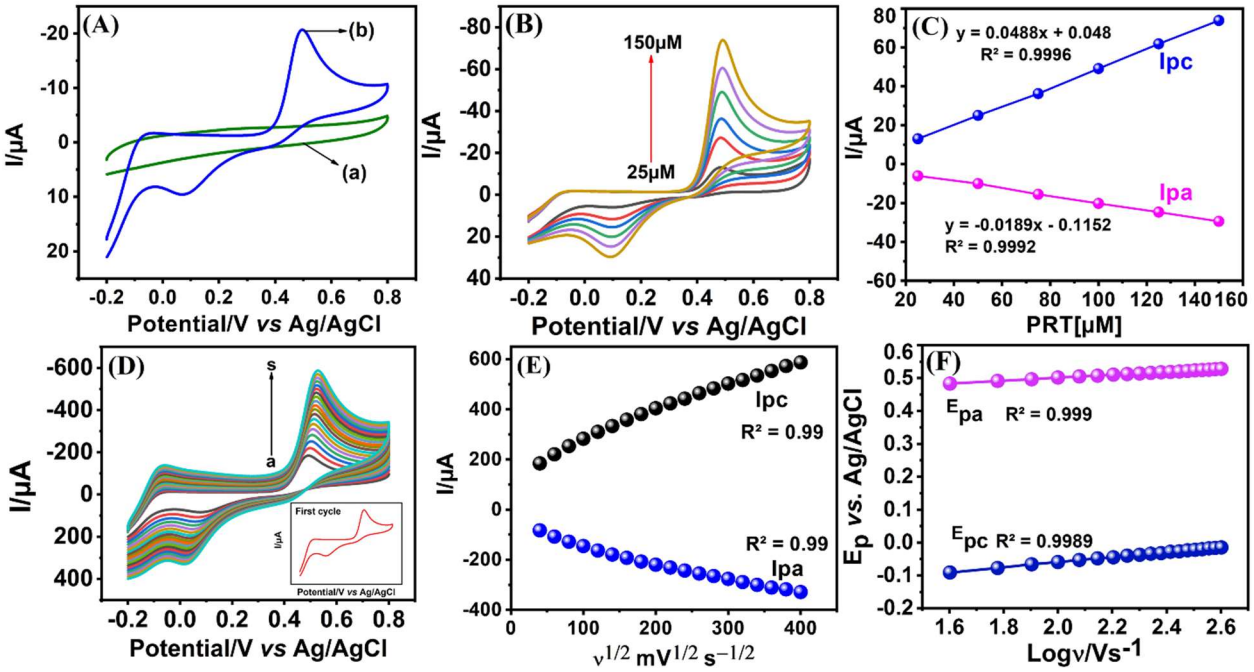

Fig.6. typical CV curves of different electrodes (such as bare GCE (a) an d CuO NWs/GCE (b)). (B) CV profiles of CuO NWs/GCE containing 20-150μM of PRT. Supporting electrolyte: 0.1M PB solution (pH 7.0) at a sweep rates $0.05Vs^{-1}$. (C) The linear relationship between peak current *vs*. concentrations. (D) Various scan rates, (E) scan rates *vs.* current relationship, (F) Log of scan rate *vs.* peak potential relationship.

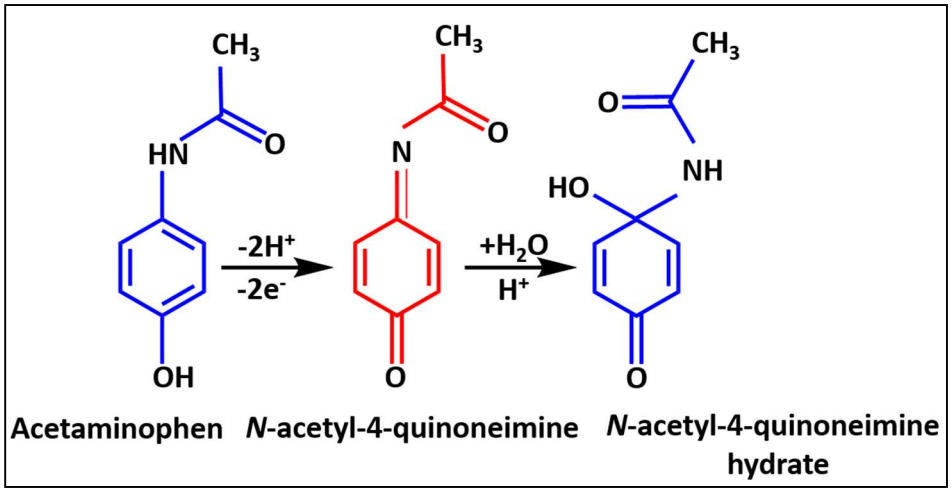

Scheme 2. Electrochemical oxidation mechanism of PRT at CuO NWs/GCE

3.5. Effect of scan rate

To further investigate the electrochemical oxidation mechanism of PRT, the effect of scan rate (ν) on the voltammetry response of PRT when CuO NWs/GCE used was studied in detail. Fig.6 (D) displays the CV analysis of CuO NWs/GCE in 0.1M PBS (pH 7.0) containing 50µM PRT (0.1mM) at a scan rates from 40 to 400 mV/s^{-1}. A notable relationship between the peak current and the square root of scan rate was observed. The linear regression equations are shown in the equations (5 and 6). Fig.6 (E) reveals that the redox reaction of PRT at the CuO NWs/GCE, which is represents a diffusion controlled process takes place. Fig.6 (F) Shows the Tafel plots for the relationship between redox potentials *vs.* log of different scan rate in seconds. The electron transfer coefficient can be calculated from the slope value. The activated complex is around halfway between reactants and products on the reaction coordinate. In other words, structure of the activated complex reflecting reactants and products equally.

$I_{pa}/A=y=-0.0065x -0.794$ $R^2 – 0.99$ → **(5)**

$I_{pc}/A=y=0.0108x +1.727$ $R^2 – 0.99$ → **(6)**

3.6. Analytical features of PRT electrochemical sensor

Fig.7 (A) displays the differential pulse voltammetry (DPV) curves obtained while using CuO NWs/GCE toward the determination of paracetamol (PRT). For various concentrations of an analyte, a well-defined DPV response was observed. The oxidation peak of PRT increases with increasing the concentrations. The plot of the oxidation current versus PRT concentrations suggested good linearity with a linear

regression of y=0.0287x + 0.2823 and R^2 = 0.99, as presented in Fig.7 (B). The obtained linear dynamic concentration range from 100nM to 275.1 µM and a sensitivity of the electrode shows 0.3632µA/μM^{-1} cm^{-2}. The limit of detection was calculated by the following equation (7);

$$\mathbf{LOD = 3S_b/S} \qquad \rightarrow \mathbf{(7)}$$

Where S_b is the standard deviation of the intercept of regression line and S is denoted as the slope of the calibration curve. From the above equation, the calculated LOD was to be 10nM. The analytical parameters such as linear working range (LWR), sensitivity and limit of detection (LOD) were compared with those in previous studies [49-59] and the comparison results are tabulated in the **Table 1**. When compared with the other modified electrodes which are presented in previous studies, the CuO NW/GC electrode is the simplest composite with higher sensitivity and a wide linear working concentration range. CuO NW/GCEs are more suitable for future commercialization due to their facile synthesis compared with the electrodes described in previous literatures.

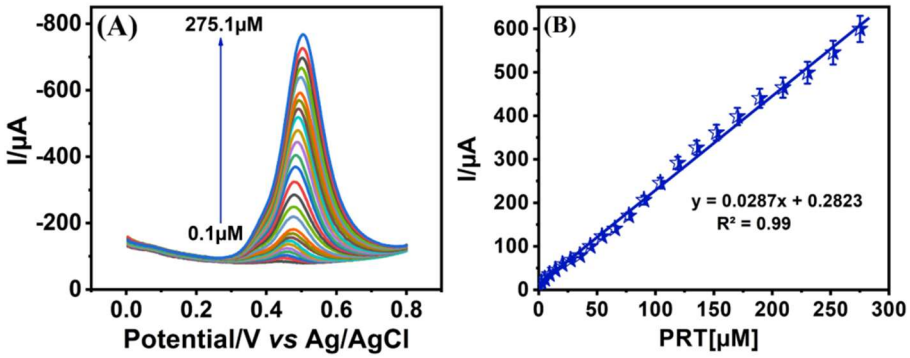

Fig.7. (A) DPVs of PRT at CuO NW /GCE and (B) corresponding linear plot for concentration *vs.* current.

Table 1. Comparison of the electrochemical sensors with current PRT sensor.

Electrodes	Technique	[j]LWR ([h] µM)	Electrolyte (pH)	[g]LOD ([i]nM)	Sensitivity (µA μM^{-1} cm^{-2})	Ref
[a]MWCNT/graphene/GCE	DPV	0.80-110.0	7.5	90	Nil	[49]

Graphene/[b]GCE	SWV	0.1-20	9.3	32	Nil	[50]
Boron-doped-diamond electrode	DPV	0.5-83	4.5	490	Nil	[51]
MWCNT/[c]PPGE	SWV	0.1-25	7.5	45	Nil	[52]
Pyrolytic carbon electrode	DPV	15-225	7.0	1400	0.33	[53]
MoS_2-[d]GR	DPV	0.1-100	5.5	20	Nil	[54]
MWCNT/chitosan	DPV	1-145	3.0	10	Nil	[55]
Carbon nanotube paste electrode	DPV	0.15-126	7.0	43	Nil	[56]
Carbon-coated-nickel nanoparticles	DPV	7.8-110	5.5	2300	Nil	[57]
Nafion/TiO_2-GR/GCE	DPV	1-100	7.0	2100	Nil	[58]
[e]PANI/ MWCNT/GCE	SWV	1-100	5.5	2500	Nil	[59]
CuO [f]NWs/GCE	DPV	0.1-275.1	7.0	10	0.3632	This work

[a]MWCNT: multi walled carbon nanotube, [b]GCE: glassy carbon electrode, [c]PPGE: plane pyrolytic graphite electrode, [d]GR: graphene, [e]PANI: poly aniline, [f]NWs: nanowires, [g]LOD: limit of detection, [h]µM: micromole, [i]nM: nanomole, [j]LWR;linear working range.

3.7. Interference, reproducibility, repeatability and stability analysis

To evaluate the anti-interference performance of the CuO NW/GCE was analyzed in presence of some oxidizing interferes such as dopamine (DA), uric acid (UA), and ascorbic acid (AA) were the results are analyzed. Fig.8 (A) describes the DPV response of the CuO NW modified electrode toward 50µM of PRT

and 20-folds higher concentration of co-existing species (above mentioned). There is no significant interference was found fro the detection of PRT. These results revealed that the electrode quickly responded to PRT (Fig.8 (B)) and interfering substances. However, very quiet responses were observed when each interfering compounds were injected separately (without paracetamol). This result suggests excellent selectivity of the electrode.

The repeatability and reproducibility were assessed in the presence of 0.1M PB solution (pH 7.0) containing 50µM of PRT, as depicted in Fig.8 (C and D). The electrode exhibits suitable repeatability with a relative standard deviation of 1.60% for five repetitive measurements conducted by using CuO NW/GCE. Moreover, the developed electrode shows good reproducibility of 1.0198% for five independent analyses.

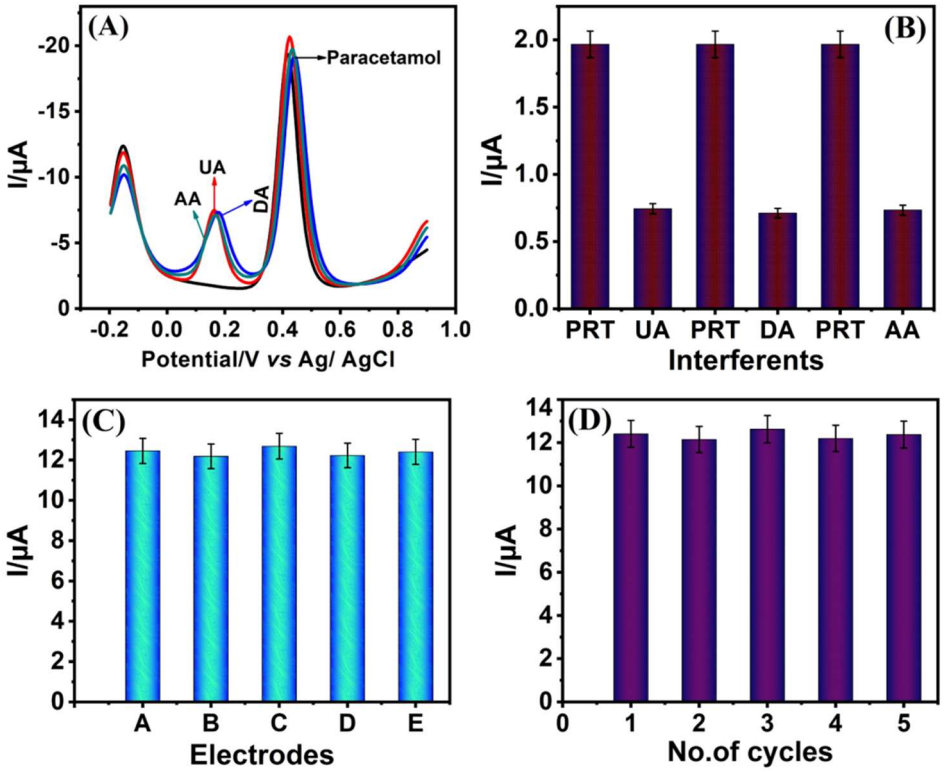

Fig.8. (A). Selectivity for the PRT at CuO NW/GCE in presence of 0.1M PB solution (pH 7.0). (B) Corresponding peak current *vs*. interfering species concentration, (C) Repeatability of PRT with five different modified electrodes and (D) Reproducibility chart for the five independent electrodes.

3.8. Real sample analysis (Bovine serum albumin)

In order to demonstrate the pragmatic applicability of the proposed sensor (PRT) were quantified in bovine serum albumin (BSA) physiological sample, on CuO NW/GCE. This sample was prepared before the experiment and three parallel determinations were carried out for this BSA detection. Table 1 presents the results. The obtained recoveries were 98.2403%, 100.90%, and 101.20% respectively for three replicate measurements with the related standard deviation was lower than 5%. Thus the obtained results prove the practical usages of the fabricated sensor in real samples.

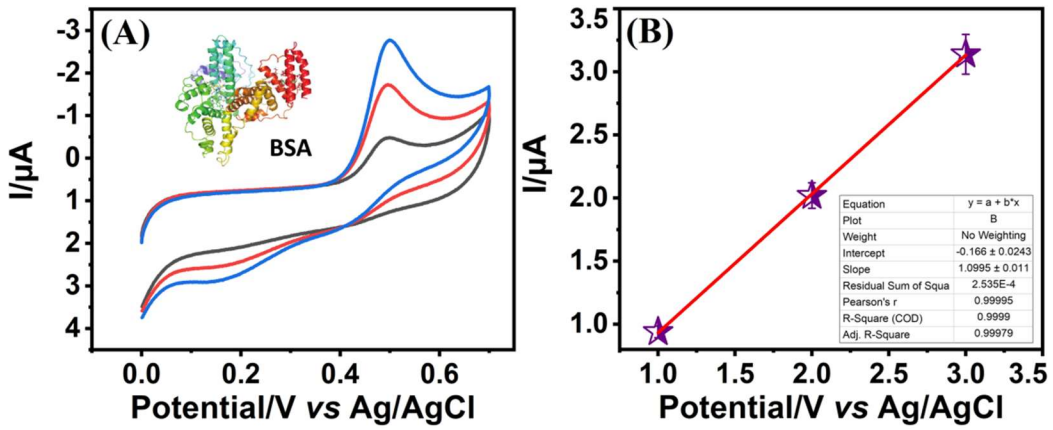

Fig.9. (A). Real sample analysis curves of PRT in BSA and (B) corresponding linear current response.

Table 2. Detection of PRT in Bovine serum albumin.

Sample	Added (μM)	Found (μM)	Recovery (%)	[a]RSD (%)
BSA	1	1.14	98.24%	2.2403%
BSA	2	2.20	100.90%	2.1514%
BSA	3	3.32	101.21%	2.8756%

4. Conclusion

To summarize the work, we have developed a technologically advanced electrochemical sensor for the effective selection and sensitization, to determine the paracetamol (PRT) which was constructed by green chemical synthesis of CuO NW electrodes using a chemical simple co-precipitation method. Morphological features of these electrode materials were appropriately characterized structurally using XRD, FTIR, EIS, and FE-SEM. The electrochemical property enhancement of the modified electrode

toward the detection of PRT was confirmed by CV and DPV analysis. The experimental results suggests that the prepared electrochemical sensor showed an excellent specificity for the quantification of PRT in presence of existence of potentially co-interfering compounds with a wide linear response range, lower limit of detection and good sensitivity. Due to this excellent behaviour, the fabricated sensor can be used for the efficient determination of PRT in pharmaceutical samples in future. Furthermore, the proposed synthesis method is simple, fast, large scale production, robust, reproducible and does not require any sophisticated instruments. In future, the present process can be further extended for the construction of various morphologies and to check their possible applications in lithium-ion batteries, fuel cells, and photocatalysis.

Conflict of interests

There are no conflicts to declare.

References

[1] T. Klinbumrung, S. Thongtem, Characterization and gas sensing properties of CuO synthesized by DC directly applying voltage, Appl. Surf. Sci. 313 (2014) 640-646.

[2] A. El-Trass, H. ElShamy, I. El-Mehasseb, M. El-Kemary, CuO nanoparticles: synthesis, characterization, optical properties and interaction with amino acids, Appl. Surf. Sci 258 (2012) 2997-3001.

[3] S. Karthick Kumar, S. Suresh, S. Murugesan, SP. Raj, CuO thin films made of nanofibers for solar selective absorber applications, Solar Energy 94 (2013) 299-304.

[4] M. Rokhmat, E. Wibowo, S. Khairurrijal, M. Abdullah, Performance improvement of TiO_2/CuO solar cell by growing copper particle using fix current electroplating method. *Proc. Eng.* 170 (2017) 72-77.

[5] N.S.K. Gowthaman, M.A. Raj, S.A. John, Nitrogen-doped graphene as a robust scaffold for the homogeneous deposition of copper nanostructures: a nonenzymatic disposable glucose sensor. *ACS Sustainable Chem Eng* 5 (2017) 1648-1658.

[6] N.S.K. Gowthaman, S.A. John, Fabrication of different copper nanostructures on indium-tin-oxide electrodes: shape dependent electrocatalytic activity. *CrystEngComm* 18 (2016) 8696-8708.

[7] L. Zhu, Y. Chen, Y. Sun, Y. Cui, M. Liang, J. Zhao, N. Li, Phase-manipulable synthesis of Cu-based nanomaterials using-ionic-liquid-1-butyl-3-methyl-imidazole tetra fluoroborate, Cryst. Res. Technol. 45 (2010) 398-404.

[8] Y.Q. Wang, D.W. Meng, X.Q. Liu, F. Li, Facile synthesis and characterization of hierarchical CuO nanoarchitectures by a simple solution route, Cryst. Res.Technol. 44 (2009) 1277-1283.

[9] C.K. Xu, Y.K. Lin, G.H. Wang, Preparation and characterization of CuO nanorods by thermal decomposition of CuC_2O_4 precursor, Mater. Res. Bull. 37 (2002) 2365-2372

[10] X.C. Jiang, T. Herricks, Y.N. Xia, CuO nanowires can be synthesized by heating copper substrates in air, Nano Lett. 2 (2002) 1333-1338.

[11] N.S.K. Gowthaman, S. Shankar, S.A. John, Ultrasensitive and selective hydrazine determination in water samples using Ag–Cu Heterostructures-Grown indium tin oxide electrode via environmentally benign methods. *ACS Sustainable Chem Eng* 6 (2018) 17302-17313.

[12] F.S. Ke, L. Huang, G.Z. Wei, L.J. Xue, J.T. Li, B. Zhang, S.R. Chen, X.Y. Fan, S.G. Sun, One-step fabrication of CuO nanoribbons array electrode and its excellent lithium storage performance, Electrochim. Acta. 54 (2009) 5825-5829.

[13] C.Y. Ma, L.J. Zhu, S.F. Chen, Y.X. Zhao, Simple and rapid preparation of CuO nanowires and their optical properties, Mater. Lett. 108 (2013) 114-117.

[14] S. Sonia, N.D. Jayram, P.S. Kumar, D. Mangalaraj, N. Ponpandian, C. Viswanathan, Effect of NaOH concentration on structural, surface and antibacterial activity of CuO nanorods synthesized by direct sonochemical method, Super lattice Microst. 66 (2014) 1-9.

[15] K.M. Shrestha, C.M. Sorensen, K.J. Klabunde, Synthesis of CuO nanorods, reduction of CuO into Cu nanorods, and diffuse reflectance measurements of CuO and Cu nanomaterials in the near infrared region, J. Phys. Chem. C.114 (2010) 14368-14376.

[16] V.K. Patel, Sonoemulsion synthesis of long CuO nanorods with enhanced catalytic thermal decomposition of potassium perchlorate, J. Clust. Sci. 24 (2013) 82-828.

[17] H.M. Xiao, L.P. Zhu, X.M. Liu, S.Y. Fu, Anomalous ferromagnetic behavior of CuO nanorods synthesized via hydrothermal method, Solid State Commun.141 (2007) 431-435.

[18] J.R. Huang, G.J. Fu, C.C. Shi, X.Y. Wang, M.H. Zhai, C.P. Gu, Novel porous CuO microrods: synthesis, characterization, and their photocatalysis property, J. Phys. Chem. Solids. 75 (2014) 1011-1016.

[19] F. Bayansal, H.A. C¸ etinkara, S. Kahraman, H.M. C. akmak, H.S. Güder, Nano-structured CuO films prepared by simple solution methods: plate-like, needle-like and network-like architectures, Ceram. Int. 38 (2012) 1859-1866

[20] Y. Zhang, X.L. He, J.P. Li, H.G. Zhang, X.G. Gao, Gas-sensing properties of hollow and hierarchical copper oxide microspheres Sens. Actuators B: Chem. 128 (2007) 293-298.

[21] L.X. Yang, Y.J. Zhu, H. Tong, L. Li, L. Zhang, Multistep synthesis of CuO nanorod bundles and interconnected nanosheets using $Cu_2(OH)_3Cl$ plates as precursor, Mater. Chem. Phys. 112 (2008) 442-447.

[22] N. Ba, L. Zhu, G. Zhang, J. Li, H. Li, Facile synthesis of 3D CuO nanowire bundle and its excellent gas sensing and electrochemical sensing properties. Sens. Actuators B 227 (2016) 142-148.

[23] F. Gao, L. Zhu, H. Li, H. Xie, Hierarchical flower-like CuO film: One-step room temperature synthesis, formation mechanism and excellent optoelectronic properties. Mater. Res. Bullet. 93 (2017) 342-351.

[24] H. Xie, L. Zhu, W. Zheng, J. Zhang, F. Gao, Y. Wang, Microwave-assisted template-free synthesis of butterfly-like CuO through $Cu_2Cl(OH)_3$ precursor and the electrochemical sensing property. Solid State Sci. 61 (2016) 146-154.

[25] A. Wade, Martindale the Extra Pharmacopia (27th ed.), The Pharmaceutical Press, London (1979)

[26] SJR. Prabakar, SS. Narayanan, Amperometric determination of paracetamol by a surface modified cobalt hexacyanoferrate graphite wax composite electrode. Talanta 72 (2007) 1818-1827.

[27] A.G. Fogg, P.J. Sausins, J.R. Smithson, The determination of paracetamol and aspirin in mixtures by nonaqueous potentiometric titrimetry or by ultraviolet spectrophotometry. Anal. Chim. Acta, 49 (1970) 342-345.

[28] K. Brandt, Paracetamol in the treatment of osteoarthritis pain. Drugs, 63 (2003) 23-41.

[29] J. Li, J. Liu, G. Tan, J. Jiang, S. Peng, M. Deng, D. Qian, Y. Feng, Y. Liu, High-sensitivity paracetamol sensor based on Pd/graphene oxide nanocomposite as an enhanced electrochemical sensing platform, Biosens. Bioelectron. 54 (2014) 468-475.

[30] S. Kesavan, S.A. John, Stable determination of paracetamol in the presence of uric acid in human urine sample using melamine grafted graphene modified electrode. J. Electroanal. Chem. 760 (2016) 6-14.

[31] J.I. Gowda, D.G. Gunjiganvi, N.B. Sunagar, M.N. Bhat, S.T. Nandi bewoor, MWCNT–CTAB modified glassy carbon electrode as a sensor for the determination of paracetamol, RSC Adv. 5 (2015) 49045-49053.

[32] A. Mao, H. Li, D. Jin, L. Yu, X. Hu, Fabrication of electrochemical sensor for paracetamol based on multi-walled carbon nanotubes and chitosan–copper complex by self-assembly technique, Talanta. 144 (2015) 252-257.

[33] H. Montaseri, P.B.C. Forbes, Analytical techniques for the determination of acetaminophen: A review. TrAC Trends in Anal. Chem. 108 (2018) 122-134.

[34] M. Lecoeur, G. Rabenirina, N. Schifano, P. Odou, S. Ethgen, G. Lebuffe, C. Foulon, Determination of acetaminophen and its main metabolites in urine by capillary electrophoresis hyphenated to mass spectrometry. Talanta 205 (2019) 120108.

[35] S. Glavanović, M. Glavanović, V. Tomišić, Simultaneous quantitative determination of paracetamol and tramadol in tablet formulation using UV spectrophotometry and chemometric methods. Spectrochim. Acta A 157 (2016) 258-264.

[36] S.C. Chaves, P.N.C. Aguiar, L.M.F.C. Torres, E.S. Gil, R.C.S. Luz, F.S. Damos, R.A.A. Munoz, E.M. Richter, W.T.P. Santos, Simultaneous determination of caffeine, ibuprofen, and paracetamol by flow-injection analysis with multiple-pulse amperometric detection on boron-doped diamond electrode. Electroanalysis 27 (2015) 2785-2791.

[37] A.J. Jeevagan, S.A. John, Electrochemical determination of caffeine in the presence of paracetamol using a self-assembled monolayer of non-peripheral amine substituted copper (II) phthalocyanine. Electrochim. Acta 77 (2012) 137-142.

[38] P. Kalimuthu, S.A. John, Selective electrochemical determination of paracetamol using nanostructured film of functionalized thiadiazole modified electrode. Electroanalysis 22 (2010) 303-309.

[39] A. Kutluay, M. Aslanoglu, An electrochemical sensor prepared by sonochemical one-pot synthesis of multi-walled carbon nanotube-supported cobalt nanoparticles for the simultaneous determination of paracetamol and dopamine, Anal. Chim. Acta. 839 (2014) 59-66

[40] S. Biswas, D. Chakraborty, R. Das, R. Bandyopadhyay, P. Pramanik, A simple synthesis of nitrogen doped porous graphitic carbon: Electrochemical determination of paracetamol in presence of ascorbic acid and p-aminophenol, Anal. Chim. Acta. 890 (2015) 98-107.

[41] X.-Y. Wu, W.-J. Niu, S. Cosnier, S.-Y. Deng, X.-J. Zhang, D. Shan, Ferricyanide confined into the integrative system of pyrrolic surfactant and SWCNTs: The enhanced electrochemical sensing of paracetamol, Electrochim. Acta. 186 (2015) 16-23.

[42] N.S.K. Gowthaman, S.A. John, Modification of a glassy carbon electrode with gold–platinum core–shell nanoparticles by electroless deposition and their electrocatalytic activity. RSC Advances 5 (2015) 42369-42375.

[43] International Centre for Diffraction Data (ICDD), Joint Committee on Powder Diffraction Standards, Diffraction Data File No. 05-0661 (2000) 12.

[44] N.S.K. Gowthaman, S.A. John, Simultaneous growth of spherical, bipyramidal and wire-like gold nanostructures in solid and solution phases: SERS and electrocatalytic applications. Cryst Eng Comm. 19 (2017) 5369-5380.

[45] P. Karuppaiah, N.S.K. Gowthaman, V. Balakumar, S. Shankar, H.N. Lim, Ultrasonic synthesis of CuO nanoflakes: A robust electrochemical scaffold for the sensitive detection of phenolic hazard in water and pharmaceutical samples. Ultrasonics - Sonochemistry 58 (2019) 104649

[46] N.S.K. Gowthaman, B. Sinduja, S.A. John, Tuning the composition of gold–silver bimetallic nanoparticles for the electrochemical reduction of hydrogen peroxide and nitrobenzene. RSC Adv. 6 (2016) 63433-63444.

[47] N.S.K. Gowthaman, S. Shankar, S.A. John, Substrate catalyzed formation of Au-Cu bimetallic nanoparticles as electrocatalyst for the reduction of dioxygen and hydrogen peroxide. J. Electroanal. Chem. 812 (2018) 37-44.

[48] N.S.K. Gowthaman, B. Sinduja, S. Shankar, S.A. John, Displacement reduction routed Au–Pt bimetallic nanoparticles: a highly durable electrocatalyst for methanol oxidation and oxygen reduction. Sustainable Energy Fuels, 2 (2018) 1588-1599.

[49] M. Arvand, T.M. Gholizadeh, Simultaneous voltammetric determination of tyrosine and paracetamol using a carbon nanotube-graphene nanosheet nanocomposite modified electrode in human blood serum and pharmaceuticals, Colloids. Surf. B, 103 (2013) 84-93.

[50] X. Kang, J. Wang, H. Wu, J. Liu, I.A. Aksay, Y. Lin, A graphene-based electrochemical sensor for sensitive detection of paracetamol, Talanta, 81 (2010) 754-759.

[51] B.C. Lourenção, R.A. Medeiros, R.C. Rocha-Filho, L.H. Mazo, O. Fatibello-Filho, Simultaneous voltammetric determination of paracetamol and caffeine in pharmaceutical formulations using a boron-doped diamond electrode, Talanta, 78 (2009) 748-752.

[52] R.T. Kachoosangi, G.G. Wildgoose, R.G. Compton, Sensitive adsorptive stripping voltammetric determination of paracetamol at multiwalled carbon nanotube modified basal plane pyrolytic graphite electrode, Anal. Chim. Acta, 618 (2008) 54-60.

[53] G.P. Keeley, N. McEvoy, H. Nolan, S. Kumar, E. Rezvani, M. Holzinger, S. Cosnier, G.S. Duesberg, Simultaneous electrochemical determination of dopamine and paracetamol based on thin pyrolytic carbon films, Anal. Methods, 4 (2012) 2048-2053.

[54] K.J. Huang, L. Wang, J Li, Y.M Liu, Electrochemical sensing based on layered MoS_2–graphene composites, Sensors and Actuators B: Chemical, 178 (2013) 671-677.

[55] H. Yin, K. Shang, X. Meng, S. Ai, Voltammetric sensing of paracetamol, dopamine and 4-aminophenol at a glassy carbon electrode coated with gold nanoparticles and an organophillic layered double hydroxide, Microchimica Acta, 175 (2011) 39-45.

[56] H. Xiong, H. Xu, L. Wang, S. Wang, Characterization and sensing properties of a carbon nanotube paste electrode for acetaminophen, Microchimica Acta, 167 (2009) 129-133.

[57] S.F. Wang, F. Xie, R.F. Hu, Carbon-coated nickel magnetic nanoparticles modified electrodes as a sensor for determination of acetaminophen, Sensors and Actuators B: Chemical, 123 (2007) 495-500.

[58] Y. Fan, J.H. Liu, H.T. Lu, Q. Zhang, Electrochemical behavior and voltammetric determination of paracetamol on Nafion/TiO_2–graphene modified glassy carbon electrode, Colloids Surf. B, 85, (2011) 289-292.

[59] M.Q. Li, L.H. Jing Electrochemical behavior of acetaminophen and its detection on the PANI–MWCNTs composite modified electrode, J. Electrochimica Acta, 52 (2007) 3250-3257.

[60] N. P. Shetti, S. J. Malode, D.S. Nayak, T.M. Aminabhavi, K.R. Reddy, Nanostructured silver doped TiO_2/CNTs hybrid as an efficient electrochemical sensor for detection of anti-inflammatory drug, cetirizine, Microchem-J, 150 (2019) 104124. https://doi.org/10.1016/j.microc.2019.104124.

[61] B. He, H. Liu, Electrochemical determination of nitrofuran residues at gold nanoparticles/graphene modified thin film gold electrode, Microchem-J, 150 (2019) 104108. https://doi.org/10.1016/j.microc.2019.104108.

[62] S.A. Rezvani, A. Soleymanpour, Application of a sensitive electrochemical sensor modified with WO_3 nanoparticles for the trace determination of theophylline. Microchem-J, 149 (2019) 104005. https://doi.org/10.1016/j.microc.2019.104005.